

# Radio Variability of Sagittarius A\* - A 106 Day Cycle

Jun-Hui Zhao

Harvard-Smithsonian CfA, 60 Garden St, MS 78, Cambridge, MA 02138

[jzhao@cfa.harvard.edu](mailto:jzhao@cfa.harvard.edu)

and

G. C. Bower & W. M. Goss

NRAO-AOC, P. O. Box 0, Socorro, NM 87801

[gbower@nrao.edu](mailto:gbower@nrao.edu) & [mgoss@nrao.edu](mailto:mgoss@nrao.edu)

Received \_\_\_\_\_; accepted \_\_\_\_\_

Submitted to ApJ Lett.

## ABSTRACT

We report the presence of a 106-day cycle in the radio variability of Sgr A\* based on an analysis of data observed with the Very Large Array (VLA) over the past 20 years. The pulsed signal is most clearly seen at 1.3 cm with a ratio of cycle frequency to frequency width  $f/\Delta f = 2.2 \pm 0.3$ . The periodic signal is also clearly observed at 2 cm. At 3.6 cm the detection of a periodic signal is marginal. No significant periodicity is detected at both 6 and 20 cm. Since the sampling function is irregular we performed a number of tests to insure that the observed periodicity is not the result of noise. Similar results were found for a maximum entropy method and periodogram with CLEAN method. The probability of false detection for several different noise distributions is less than 5% based on Monte Carlo tests. The radio properties of the pulsed component at 1.3 cm are spectral index  $\alpha \sim 1.0 \pm 0.1$  (for  $S \propto \nu^\alpha$ ), amplitude  $\Delta S = 0.42 \pm 0.04$  Jy and characteristic time scale  $\Delta t_{FWHM} \approx 25 \pm 5$  days. The lack of VLBI detection of a secondary component suggests that the variability occurs within Sgr A\* on a scale of  $\sim 5$  AU, suggesting an instability of the accretion disk.

*Subject headings:* Galaxy:center — accretion, accretion disks — galaxies:active — radio continuum: galaxies — black hole physics — radio source: Sgr A\*

## 1. Introduction

The compact radio source Sagittarius A\* is suggested to be associated with a supermassive black hole at the Galactic Center (Eckart & Genzel *et al.* 1997, Ghez *et al.* 1998, Backer & Sramek 1999, Reid *et al.* 1999). The flux density variability of Sgr A\* has been puzzling since the discovery of this intriguing radio compact source at the center

of the Galaxy in 1974 (Brown & Lo 1982; Zhao *et al.* 1989). We monitored Sgr A\* with the VLA during the period of 1990 to 1993. Fluctuations in flux density suggested that the amplitude of variation increased towards short wavelengths and that the rate of outbursts is about three per year (Zhao *et al.* 1992; Zhao & Goss 1993). Large amplitude fluctuations in the flux density have been observed at millimeter wavelengths (Backer & Wright 1993; Tsuboi *et al.* 1999). Based on the radio monitoring data obtained with the 3.5 km Green Bank Interferometer at 11 and 3.6 cm, Falcke (1999) reported that at both wavelengths a characteristic time scale of 50 to 200 days is observed while the structure function of 11 cm data suggests a quasi-periodic variation with a period of 57 days.

## 2. Observations & Data Reduction

Regular observations were made during 1990.1-1991.5 with various sampling intervals in a range from 1 day to 28 days at 3.6, 2 and 1.3 cm in the A, B, C, D and the hybrid configurations of the VLA. Less regular observations at the same frequencies were made at the same frequencies between 1991.5 and 1993.5. The largest gap between observations in these data was 120 days. In addition to these regularly sampled data from 1990 to 1993 discussed previously by Zhao *et al.* 1992, we have collected all the observations of Sgr A\* at 20, 6, 3.6, 2 and 1.3 cm from the VLA archive for the past two decades. We accepted only the observations with baselines long enough ( $> 80k\lambda$ ) to separate Sgr A\* from the extended HII emission. This limit corresponds to 3" resolution.

Primary flux density calibration was performed in the standard way using 3C 48 or 3C 286. The flux density scale was then bootstrapped to one of several nearby compact radio sources, typically J1733-130, J1744-312 or J1751-253. Most of the flux densities presented in this paper were determined in the visibility domain, from the long baseline data. In a few cases in which the length of baselines was marginal in separating the point source in

the visibility domain we determined the flux densities of Sgr A\* in the image plane. Then, the flux density of Sgr A\* was measured by subtracting the confusion from the extended emission. In the cases in which the telescope pointing was offset from Sgr A\*, both the primary beam and synthesis beam effects are corrected.

Figure 1 shows the radio light curves at the five wavelengths for Sgr A\*. At all wavelengths determination of the absolute flux density scale dominates the errors. There are also contributions due to the thermal noise, separation from the extended HII region Sgr A West for low angular resolution data and uncertainty in the atmospheric opacity at 2 and 1.3 cm. Uncertainty at long wavelengths is less than 5%. For long tracks, this uncertainty can be minimized by removing the attenuation of the gain as a function of elevation. The correction for this effect is no more than 10% at 1.3 cm based on several observations with 8 hr tracking time. Most of the observations used in this paper were in a snapshot mode (10-20 minutes in integration). For these short observations, we can assess the uncertainty based on observations of a stable, nearby ( $4^\circ$  away from Sgr A\*) calibrator J1751-253 (Figure 1b). The 7% fluctuation of the flux density at 1.3 cm for J1751-253 reflects the uncertainty in the calibration.

### 3. Data Analysis & Results

#### 3.1. Power Spectrum and A Period of 106 Day

We carried out a power spectral density (PSD) analysis of the light curves in order to identify periodic signals. With a simple Fourier analysis, the irregular sampling of the VLA archive data produces strong side-lobes, leading to confusion in the identification of spectral features. In addition large gaps in the sampling can produce an alias of a periodic signal to lower frequency lags, weakening the power of the true signal and producing aliased signals.

To minimize the side-lobes, we estimated the PSD with the maximum entropy method (MEM) (Press *et al.* 1989) and with a classic periodogram augmented with CLEAN. The results from both approaches are completely consistent.

In order to overcome the aliasing problem due to large gaps in time, we used the following procedure. This procedure determines the period from well-sampled but small data set, folds an irregularly-sampled but larger data set with that period and then searches for a new period. We considered three subsets of the full light curves: 1990-91, 1990-93 and 1977-1999 (*i.e.*, the full set). We removed a third-order polynomial from each of these data sets. This baseline represents slow variations in the flux density of Sgr A\*. In the 1990-91 subset, the maximum sampling gap (28 days) corresponds to the Nyquist critical frequency of  $f_c = 2.1 \times 10^{-7}$  Hz. Using the zero-leveled subset 1990-91, we calculated a PSD profile. At 1.3 cm, we found a spectral peak at the frequency  $f = 1.07 \times 10^{-7}$  Hz, corresponding to a period  $P = 107$  days. This frequency is well within the range of Nyquist critical frequency.

To verify the periodic signals, we examined the 1990-93 and 1977-99 subsets folded into  $N_{cyc}$  cycles of period  $P_{in}$ . The 1990-93 consists of 59 observations during the period 1990.1-1993.8, containing  $\sim 1/2$  of the total data points in 1977-99. The maximum gaps in the sampling are 120 and 1350 days for the subsets 1990-93 and 1977-99, respectively. The number  $N_{cyc}$  is chosen as the largest number such that the maximum sampling gap ( $\Delta t_{max}$ ) in the new folded time series is smaller than half the value of the period. Taking the new folded time series of these subsets, we calculate PSD profiles. Table 1 and Figure 2 summarize the results. The peak frequencies ( $f$ ) derived from these three data sets are consistent, with a mean value of  $1.09 \times 10^{-7}$  Hz. The uncertainty  $\sigma_f \sim 3 \times 10^{-9}$  Hz (3 days) of the peak frequency is estimated from the maximum deviation of the peak frequencies derived from the three data subsets. The FWHM width ( $\Delta f$ ) of the PSD feature is  $9 \times 10^{-8}$  Hz derived from both 1990-91 and 1990-93 subsets. For the 1977-99 subset, the FWHM

width is reduced by a factor of 2 ( $\Delta f = 5 \times 10^{-8}$  Hz). The uncertainty of the FWHM width due to noise and the irregular sampling is  $\sim 15\%$ . The ratio of  $f/\Delta f$  is  $\sim 2.2 \pm 0.3$ .

For the 2 cm data, we followed the same procedure. The mean peak frequency is consistent with the result obtained from 1.3 cm. The power spectral feature derived from all the data at 2 cm appears to be broadened by a factor of  $\sim 2$  as compared to that of 1.3 cm. The ratio of  $f/\Delta f$  is  $\sim 1.0 \pm 0.2$  at 2 cm.

At 3.6, 6 and 20 cm we folded the data with a period of 106 days. We used two subsets of the data for the 3.6 cm data, 1990-1993 and 1988-1999, and the whole data sets for the 6 and 20 cm data. At 3.6 cm a spectral feature with a period of 106 days is marginally detected. This feature has a ratio of peak frequency to width  $f/\Delta f < 0.4$ . No significant features are detected in the 6 and 20 cm data.

Using the procedure discussed above, we also folded the 1.3 cm data into a number of cycles with a small period to check if the PSD feature observed is an aliased signal from a higher frequency periodic variation. We have checked the periods ranging between 1 to 56 days which is outside the highest Nyquist frequency  $f_c = 2.1 \times 10^{-7}$  Hz provided by the VLA observations. No spectral features from the folded data sets are stronger and narrower than the  $1 \times 10^{-7}$  Hz feature. No periodic signals from the calibrator J1751-253 is found confirming that the periodic variation is not caused by calibration errors.

There is a probability that the periodic signal discussed above could be a false detection due to a combination of a random process and the irregular sampling function. To provide a quantitative estimate, we have carried out Monte Carlo tests with data sets created from various noise sources using the sampling function of the real data and the procedure outlined above. Our noise functions included white noise, Gaussian noise around a mean and a Poisson distribution of flares. These flares were modeled as  $\delta$  function rises in flux density that occurred with a probability  $p$  and decayed with an exponential time constant

$t_d$ . We searched the ranges  $0.001 < p < 0.27$  and  $1 < t_d < 90$  days. We also considered sets of data in which we reordered (or scrambled) the actual measured flux densities. This test assumes no knowledge of the parent distribution of the flux density. Based on the 1990-93 data at 1.3cm, we find that the probability of false detection due to a random process is less than 5% for all of these cases. False detection occurs when the ratio  $f/\Delta f$  of the noise data set exceeds that of the true data set with the same sampling function.

### 3.2. The Mean Profiles of the 106 Day Cycle

Figure 3 shows the mean profiles of the 106 day cycle constructed by folding the time series data (1990.1-1993.8) into a 106 day period. Again, the long term baselines were removed before folding. The zero levels reflect the mean flux densities of Sgr A\* as listed in the caption to Figure 1. The 0-phase in the plots corresponds to a reference day (4 Dec 1991). Because of the uncertainty in period (3% from the 1.3 cm data), the phase uncertainty for folding long time baseline data becomes large. The maximum uncertainty of the phase in the mean profile for the period 1990.1-1993.8 is  $\sim 20$  days. The radio properties of the 106 day cycle are summarized in Table 1. Both the absolute ( $\Delta S$ ) and fractional ( $\Delta S/S$ ) amplitudes of the “pulsed” component appear to increase towards short wavelengths. The mean spectral index in the “pulsed” component is  $\alpha \approx 1.0 \pm 0.1$  ( $S \propto \nu^\alpha$ ). The phase transition from minimum to maximum appears to be sharper at 1.3 cm than 2 cm, although we could not observe any significant phase offsets. The FWHM ( $\Delta t \pm \sigma_{\Delta t}$ ) of the mean profile is roughly  $25 \pm 5$  and  $40 \pm 10$  days for 1.3 and 2 cm, respectively. There are multiple peaks in the 3.6 profile indicating the typical time scale ( $\Delta t$ ) of individual periodic events is comparable to the the period (106 days) at this wavelength. In addition, the FWHM width of the periodic feature increases as the wavelength increases as shown in Figure 2. The periodic fluctuation appears to diminish at the longer wavelengths.

#### 4. Discussion

If the 106 day cycle is related to an orbital emitting object around the massive black hole, its distance to the central mass would be  $1200 \times R_g$  (60 AU), where  $R_g = 7.5 \times 10^{11}$  cm for  $2.5 \times 10^6 M_\odot$ . At a distance of 8 kpc, 60 AU corresponds to 8 mas. A 200 mJy compact object separated by 8 mas from Sgr A\* is easily detected with the VLBA at wavelengths shorter than 3.6 cm. There is no evidence for a companion source in images of Sgr A\* at any wavelength (e.g., Bower & Backer 1998). We can also demonstrate the unlikelihood of the specific case of an eccentric binary pair in which a wind from the secondary eclipses the primary as in the case for the pulsar PSR 1259-63 (Johnson *et al.* 1992). The opacity of free-free absorption  $\tau_{f-f} \sim \lambda^{2.1}$  suggests that the periodic variability due to an orbiting body would be enhanced at longer wavelengths. At  $\lambda \geq 6$  cm, Sgr A\* would be completely absorbed in the eclipsed phase if  $\tau \sim 0.5$  as inferred from the fraction of 40% in the flux density variation at 1.3 cm. Thus, the periodic variability is more likely intrinsic to Sgr A\* and probably occurs within a few hundred  $R_g$  of the massive black hole.

Quasiperiodic variability in radio flux density can be produced through jets or collimated flows. With a wealth of data observed at wavelengths between radio to X-ray, the microquasar GRS 1915+105 provides an excellent case showing two distinct states (“plateau” and “flare”) of the accretion process in a stellar mass black hole, (Mirabel & Rodriguez 1999; Dhawan *et al.* 2000). The current state of Sgr A\* is similar to the “plateau” state of GRS 1915+105 in terms of flat radio spectrum, compact source size (AU scale) and periodic variability in radio flux density. This state can be contrasted to the “flare” state which is characterized by optically thin ejecta feeding large scale jets (500 AU). The radio variability as correlated with the soft X-ray cycle in the “plateau” state of GRS 1915+105 suggests that the radio oscillations correspond to the thermal-viscous instability of the accretion disk (Dhawan *et al.* 2000). The analog of the radio fluctuations in the two

sources suggests that the periodic flux density variations in Sgr A\* are also related to an instability of the accretion disk. However, the X-ray luminosity ( $\sim 2 \times 10^6 L_\odot$ ) of GRS 1915+105 is 20 times greater than the Eddington limit for a  $3 M_\odot$  black hole (Mirabel & Rodriguez 1999) and the radio jets are produced by the overwhelming radiation pressure. On the other hand, the low X-ray luminosity ( $< 100 L_\odot$ ,  $\sim 10$  orders in magnitude below the Eddington limit for a  $2.5 \times 10^6 M_\odot$  object) of Sgr A\* indicates that the gravity far exceeds the radiation pressure. Because of the strong gravity and weak radiation pressure, the consequence of the gas dynamics in Sgr A\* on the AU scales would be different from GRS 1915+105. In fact, the time variability and the limit on the intrinsic source size ( $< 0.5$  mas or  $100 R_g$  or 5 AU) of Sgr A\* from the 7 mm observations (Lo *et al.* 1998 and Bower and Backer 1998) suggest that any variability in the jet occurs in a region where the gravitational field of the black hole dominates. Any collimations of jets or outflows related to the observed radio variability appear to be disrupted within Sgr A\* on a scale of  $\sim 5$  AU. A model consisting of a jet nozzle (*e.g.* Falcke 1996) seems useful to study if a self-consistent dynamic theory for the disk instability can be constructed.

A convection process is now considered in the advection dominated accretion flow (ADAF) that could well provide a reasonable dynamic model for the accretion disk and possible outflows (Narayan *et al.* 2000; Quataert & Gruzinov 2000; Igumenshchev & Abramowicz, 1999; Stone *et al.*, 1999). In this theory, hot dense bubbles are produced in the inner part of a low-viscosity disk through convection caused by thermal instability. The most attractive result from the convective-ADAF theory is that quasiperiodic production of convective bubbles has been observed in numerical simulations, although the observed period and the small cycle frequency width have not been predicted in detail from the theory (Igumenshchev & Abramowicz, 1999). The current results appear to favor the convective-ADAF model although we can not rule out the possibilities of an orbiting companion object that triggers periodic flares from a jet nozzle.

We thank Ramesh Narayan for stimulating discussion concerning the convective ADAF model, and Ron Ekers for his helpful discussion and his initial suggestion of the VLA monitoring program in 1980. We thank Don Backer for helpful discussions and Heino Falcke for sharing recent data from the GBI. The Very Large Array (VLA) is operated by the National Radio Astronomy Observatory (NRAO). The NRAO is a facility of the National Science Foundation operated under cooperative agreement by Associated Universities, Inc.

## REFERENCES

Backer, D. C. and Sramek, R. A. 1999, ApJ, 524, 805

Backer, D. C. and Wright, M. 1993, ApJ, 417, 560

Bower, G. C. and Backer, D. C. 1998, ApJ, 496, L97

Brown, R. L. and Lo, K. Y. 1982, ApJ, 253, 108

Dhawan, V., Mirabel, I. F. and Rodriguez, L. F. 2000, ApJ, 543, 1 nov 2000 issue

Eckart, A., and Genzel, R. 1997, MNRAS, 284, 576

Falcke, H. 1996 in IAU Symp. 169, p163

Falcke, H. 1999 in ASP Conf. Series 186, p113

Ghez, A. M., Klein, B. L., Morris, M., and Becklin, E. E. 1998, ApJ, 509, 678

Igumenshchev, I. V. and Abramowicz, M. A. 1999, MNRAS, 303, 309

Johnston, S., Manchester, R. N., Lyne, A. G., Bailies, M., Kaspi, V. M., Qiao, G., and D'Amico, N. 1992, ApJ, 387, L37

Lo, K. Y., Shen, Z., Zhao, J.-H. and Ho, P. 1998, ApJ, 508, L61

Mirabel, I. F. & Rodriguez, L. F. 1999, ARA&A, 37, 409

Narayan, R., Igumenshchev, I. V. and Abramowicz, M. A. 2000, ApJ, 539, 798

Press, W. H., Flannery, B. P., Teukolsky, S. A. and Vetterling, W. T. 1988, Numerical Recipes, Cambridge University Press

Quataert, E. and Gruzinov, A. 2000, ApJ, 539, 809

Reid, M. J., Readhead, A. C. S., Vermeulen, R.C., & Treuhaft, R. N. 1999, ApJ, 524, 816

Stone, J. M., Pringle, J. M., & Begelman, M. C. 1999, MNRAS, 310, 1002

Tsuboi, M., Miyazaki, A. & Tsutsumi, T. 1999, ASP Conf. Series 186, p105

Zhao, J.-H., Ekers, R. D., Goss, W. M., Lo, K. Y. and Narayan R. 1989, IAU Symp. 136, 535.

Zhao, J.-H., Goss, W. M., Lo, K. Y. and Ekers, R. D. 1992, ASP Conf. Series 31, 295

Zhao, J.-H. and Goss, W. M. 1993 Sub-arcsecond Radio Astronomy, R.J. Davis and R. S. Booth, Cambridge University Press, 38

Fig. 1.— a. (left panel) The radio light curves of Sgr A\* observed with the VLA at 20, 6, 3.6, 2, 1.3 cm over the past two decades. The solid lines connect two successive data points (dots). The vertical error bar indicates  $1\sigma$ . The dotted curves indicate the third-order polynomial baselines which are removed from the data prior to the periodic analysis as discussed in Table 1 and Figures 2 and 3. b. (right panel) The radio light curves of Sgr A\* (filled dots) and a calibrator J1751-253 (open circles) observed during 1990-1993. The calibrator J1751-253 is a compact (less than 0.1 arcsec), steep spectrum source. The flux density of J1751-253 was stable in this period as compared with those of Sgr A\*. The mean flux density and standard deviation ( $S \pm \delta S$ ) are  $1.20 \pm 0.01$ ,  $0.470 \pm 0.009$ ,  $0.278 \pm 0.005$ ,  $0.157 \pm 0.007$ ,  $0.116 \pm 0.008$  Jy for J1751-253 and  $0.513 \pm 0.049$ ,  $0.710 \pm 0.072$ ,  $0.783 \pm 0.099$ ,  $0.99 \pm 0.18$ ,  $1.10 \pm 0.23$  Jy at 20, 6, 3.6, 2, 1.3 cm for Sgr A\* during this period.

Fig. 2.— The power spectral density profiles derived from all the data folded into 6 cycles of the period 106 days at each wavelength. Each profile along the vertical axis is normalized by its peak value and is modified by adding 0, 0.5, 0.75, 1.5 and 2.0 at 1.3, 2, 3.6, 6 and 20 cm, respectively. A peak near  $1 \times 10^{-7}$  Hz is clearly detected at 1.3, 2 cm while the detection at 3.6 cm is marginal ( $< 3\sigma$ ). The width of the spectral feature increases as the wavelength increases. No significant periodicities from the 20 and 6 cm data were detected.

Fig. 3.— The mean profiles of the 106 day cycle at 3.6, 2 and 1.3 cm are obtained by folding the data obtained during 1990.1-1993.8 (Figure 1b) into one single cycle. The profiles are smoothed. The mean spectral index of the “pulsed” components is about  $\alpha \sim 1$  ( $\Delta S \propto \nu^\alpha$ ). The long-term baseline (the third-order polynomial) has been taken out in the PSD fitting and cycle folding processes. The zero levels here reflect the mean flux densities of Sgr A\* as listed in the captions to Figure 1b.

Table 1. The Results of Power Spectral Fitting for Sgr A\*

| $\lambda$<br>(cm) | $f$ ( $\sigma_f$ )<br>( $10^{-7}$ Hz) | $\Delta f$ ( $\sigma_{\Delta f}$ )<br>( $10^{-7}$ Hz) | $f/\Delta f(\sigma_{f/\Delta f})$ | $P$ ( $\sigma_P$ )<br>(day) | $\Delta S(\sigma_{\Delta S})$<br>(Jy) | $\Delta S/S(\sigma_{\Delta S/S})$<br>(%) | $\Delta t$ ( $\sigma_{\Delta t}$ )<br>(day) |
|-------------------|---------------------------------------|---|-----------------------------------|-----------------------------|---------------------------------------|--|---|
| 1.3               | 1.09 (0.03)                           | 0.50 (0.07)   | 2.2 (0.3)                         | 106 (3)                     | 0.42 (0.04)                           | 34 (9)                                   | 25 (5)                                      |
| 2.0               | 1.12 (0.10)                           | 0.80 (0.12)   | 1.0 (0.2)                         | 104 (9)                     | 0.28 (0.02)                           | 25 (6)                                   | 40 (10)                                     |
| 3.6               | 1.10 (0.01)                           | >3  | <0.4                              | 106 (1)                     | 0.16 (0.01)                           | 20 (4)                                   | ~100  |

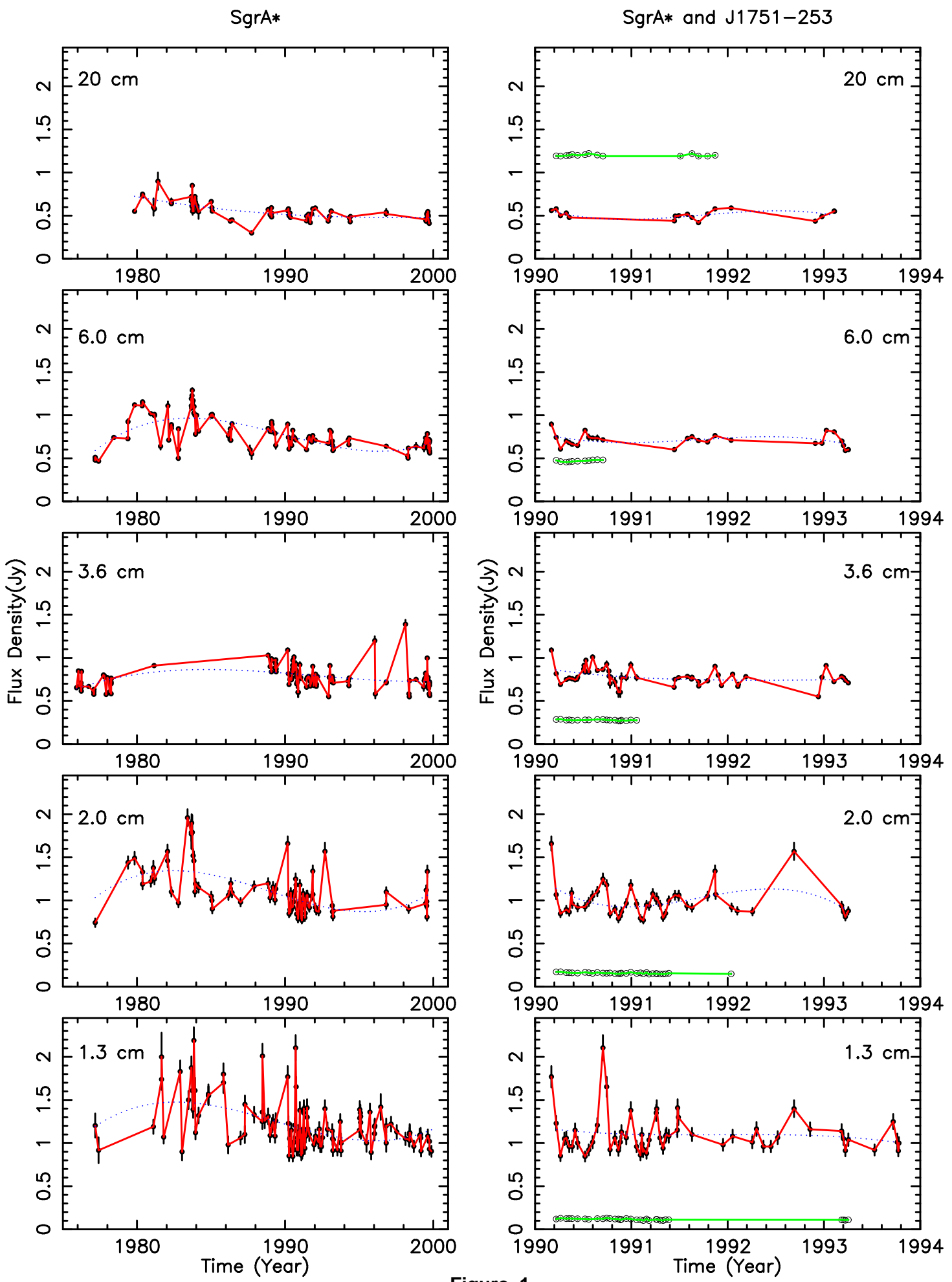
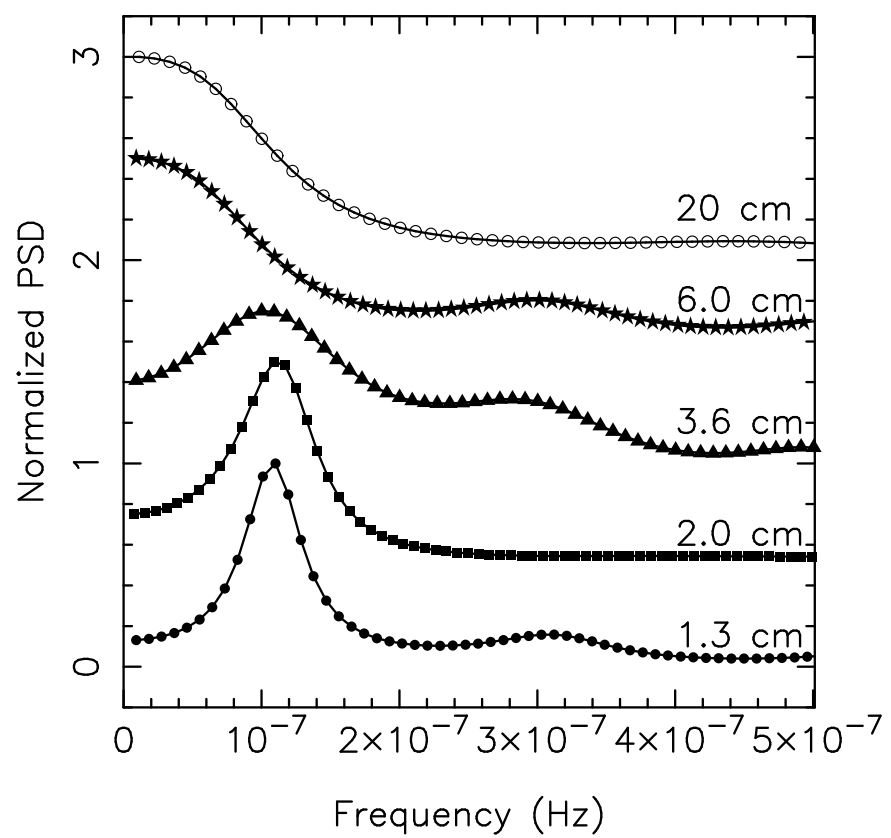
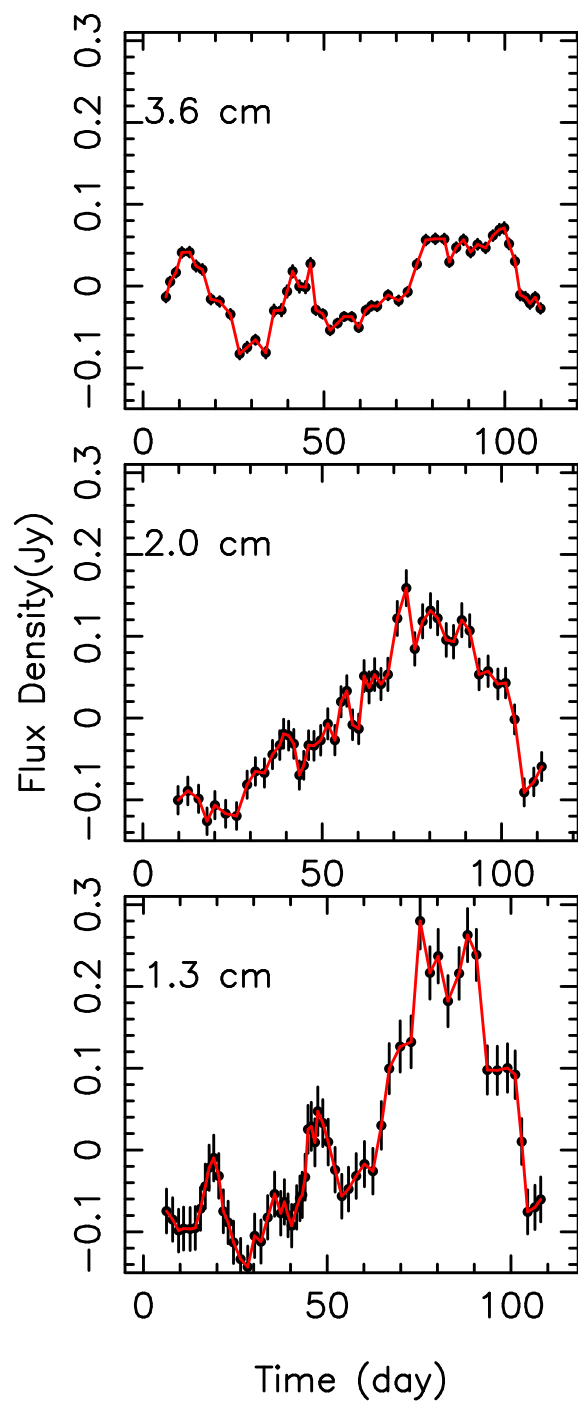


Figure 1



**Figure 2**



**Figure 3**